CrossMark

Effect of Microstructure on Corrosion Behavior of Mg–Sr Alloy in Hank's Solution

Jia-Hui Dong[1,2] · Li-Li Tan[1] · Yi-Bin Ren[1] · Ke Yang[1]

Abstract

Mg–Sr alloy has been studied as a potential biodegradable material with excellent bioactivity to promote the bone formation. However, its degradation behavior needs to be well controlled to avoid the negative effect, which is important for future application. Therefore in this study, the microstructure and its effect on corrosion behavior of an Mg–1.5Sr alloy were investigated. The microstructures of the alloy under different processing procedures were characterized by both optical and scanning electron microscopes. The corrosion performance was studied in Hank's solution using immersion, potentiodynamic polarization and electrochemical impedance spectroscopy (EIS) tests. The results showed that the grain size and the amount and distribution of β-Mg$_{17}$Sr$_2$ had obvious effects on the corrosion behavior of Mg–Sr alloy. The smaller the grain size was, the more the protective surface layer formed on Mg–Sr alloy, and the higher the corrosion resistance was. For the as-cast Mg–Sr alloy, the network-like second phases precipitated along the grain boundaries could not hinder the corrosion due to their own corrosion cracking accelerating the intergranular corrosion. However, the refinement of second phases increased the corrosion resistance of the as-extruded alloy. After solution treatment at 450 °C for 5 h, the grains in the alloy did not grow much and β-Mg$_{17}$Sr$_2$ phases homogenously distributed in the alloy, resulting in the increase in corrosion resistance. However, after aging treatment, large amount of precipitated second phases increased the galvanic corrosion of the alloy, accelerating the development of corrosion.

1 Introduction

Biodegradable metals are attracting much attention in recent years. As the conventional medical metals, such as stainless steel, titanium alloy and Co–Cr alloy, have risks of local inflammations caused by metal implantations. Magnesium (Mg) alloys have been found to own obvious advantages including biodegradability to avoid the secondary surgery, elastic modulus close to natural bone, excellent biocompatibility, etc. It has been reported that Mg ions could stimulate the osteogenic differentiation of stem cells in periosteum to promote bone formation; thus, magnesium alloys are attractive to be a new class of bone implant materials with prospective clinical applications [1–3]. However, in the short- or even long-term implantation the other metal ions released from the magnesium alloy during degradation may cause toxic reaction to the surrounding tissues. For example, AZ91 and WE43 magnesium alloys containing either Al or rare earth metals are widely studied due to their good corrosion resistances. However, medical studies reported that Al could cause neurotoxicity and even Alzheimer's disease, and rare earth metals could have potential cytotoxicity [4, 5]. From the viewpoint of bio-safety, some biocompatible elements including Ca, Zn, Mn have been added to develop the bio-safer Mg alloys for medical application [6–8].

As a necessary trace element, strontium (Sr) belongs to the II group in the periodic table of elements, with similar chemical and biological properties as Ca. Sr has functions of promoting osteoblast formation and inhibiting osteoclast growth [6], and the strontium salt is taken orally in clinic to

✉ Li-Li Tan
  lltan@imr.ac.cn

1 Institute of Metal Research, Chinese Academy of Science, Shenyang 110016, China

2 School of Materials Science and Engineering, University of Science and Technology of China, Shenyang 110016, China

treat the patients with osteoporosis in order to increase the bone mass and reduce the risk of fracture. It was reported that the addition of Sr in Mg alloy could increase both mechanical properties and corrosion resistance in saline solution [7]. Our previous work found that the Mg–1.5Sr alloy exhibited good cytocompatibility and better effect on osteoblast proliferation and differentiation than pure Mg [8]. Gu et al. [9] also found that the degradation of the hot-rolled Mg–Sr alloy kept steady and continuous release of Sr ions. The hot-rolled Mg–2Sr alloy was further implanted in the distal femur of rat, and there was no negative effect after 4 weeks of implantation, with a role of promoting bone mineralization. These studies indeed indicated the possibility of Mg–Sr alloy as a new bone implant material. However, we still found that the rapid corrosion of Mg–Sr alloy led to mass hydrogen evolution and alkalization environment, which may delay the healing of bone defects and result in the necrosis of tissues. Gu et al. [9] also pointed that Mg–Sr alloy still could not meet the requirement for clinical application due to its fast degradation. In fact, poor corrosion resistance in biological environment is the main obstacle for all the Mg alloys to be used as biodegradable bone implants [4, 5, 10–12]. Therefore, further improving the corrosion resistance of the Mg–Sr alloy is necessary for its future application in clinic.

The corrosion behavior of a given Mg alloy mainly depends on its microstructure (α-Mg and β-phases) as well as the surrounding environment. The microstructure of magnesium alloy can vary with the processing method including hot deformation, heat treatment, etc., presenting different corrosion behaviors. Many studies [13–15] have shown the important effect of grain size on corrosion rate of magnesium alloys. A reduction in grain size could give an increase in boundary density, which affects the dissolution and passivation of Mg alloy [13]. However, there were many arguments about the effect of grain boundary on the corrosion behavior of magnesium alloys. Aung and Zhou [13] proposed that the grain boundary could be an obstacle to the corrosion. It was reported that the magnesium alloy with refined grains appeared to possess a more pseudo-protective oxide layer on its surface, which can better protect the substrate [16]. Zeng et al. [17] found that the fine-grained microstructure in Mg–Li–Ca alloy improved the corrosion resistance of alloy and shifted the pitting corrosion to overall corrosion. The corrosion behaviors were also found to be much influenced by the second phases in Mg alloys. The second phases in Mg alloys can play a dual role, as a cathode of the galvanic corrosion to accelerate the corrosion process, or as an obstacle to reduce the corrosion development, which is related to the amount and distribution of second phases [18–22]. If the β phase is nearly continuous like a net over the α matrix and is stable in the microstructure of magnesium alloy, being inert to corrosion attack, it should have a beneficial effect to reduce the corrosion development [23]. In addition, Zeng et al. [17] also found that a greater dispersion of second phases led to relatively smaller and shallower corrosion pits and improved the corrosion resistance of Mg alloys. Therefore, the corrosion resistance of magnesium alloys can be largely related to their microstructures. However, the relation between microstructure and corrosion behavior for Mg–Sr alloy and even the corrosion mechanism of the alloy are still lack of study in depth, although there are several reports about the characterization of biodegradation behavior of Mg–Sr alloy.

Based on the previous work [8], this study was aimed to examine the corrosion mechanism in order to improve the corrosion resistance of the Mg–1.5Sr alloy through investigating the relationship between microstructure and corrosion behavior of the alloy in the simulated body fluid.

2 Material and Experiments

2.1 Material

High-purity Mg (99.95%) and Mg–25 wt%Sr master alloy were used to fabricate a cast Mg–1.5Sr alloy for studies. Its chemical composition was analyzed by inductive coupled plasma (ICP) as 1.5 wt%Sr, < 0.001 wt%Fe, < 0.001 wt%Ni, and Mg in balance. Cast Mg–1.5Sr samples were cut from the alloy ingot, marked as "as cast." The ingot was preheated at 200 °C for 2 h and then was extruded into 10-mm-diameter bars under conditions of extrusion temperature of 200 °C, extrusion ratio of 64:1 and extrusion rate of 0.3 mm s^{-1}. The transverse samples cut from bars perpendicular to the extrusion direction were marked as "as ex-t," and the longitudinal samples along the extrusion direction were marked as "as ex-l." Samples cut from the extruded bars were marked as "as extruded." The extruded Mg–1.5Sr alloy was heated at 450 and 560 °C for 5 h, respectively, followed by water quenching, in order to dissolve the second phases into the matrix, which were marked as "T4-450 °C" and "T4-560 °C." The Mg–1.5Sr alloy after solution treatment at 560 °C for 5 h was aged at 200 °C for 10–40 h, followed by air cooling, which were marked as "T6-10 h," "T6-24 h" and "T6-40 h." The heat treatment procedures of the studied Mg–1.5Sr alloy are listed in Table 1.

The samples were ground by SiC sand papers of 400#, 800#, 1200# and 2000# successively and then were polished by 0.5-μm size of Al_2O_3 polishing solution to the bright surface without obvious scratches. The polished samples were cleaned by deionized water, dried and etched for 2 s by an etching agent (picric acid 1.5 g, glacial acetic

Table 1 Heat treatments for as-extruded Mg–Sr alloy

Sample	Solution treatment		Aging treatment	
	Temperature (°C)	Time (h)	Temperature (°C)	Time (h)
T4-450 °C	450	5	–	–
T4-560 °C	560	5	–	–
T6-10 h	560	5	200	10
T6-24 h	560	5	200	24
T6-40 h	560	5	200	40

acid 5 ml and alcohol 10 ml). Both optical microscope and scanning electron microscope (SEM) were used to examine the microstructure, and Sisc IAS image software was employed to calculate the grain size and percentage of second phases. X-ray diffractometer (XRD) using Cu K_α from 10° to 80° was employed to analyze the compositions in Mg–1.5Sr alloy under different treatments.

2.2 Immersion Test

The samples were immersed in the Hank's balanced salt solution for 14 d with an immersion ratio of 1.25 cm^2 ml^{-1}, which was then placed in a 37 ± 0.5 °C incubator. The immersion solution was refreshed once a day. The pH of the solution in tubes was measured each day during the first 3 d and measured every other day after 3 d. Three parallel samples were used for each result.

The weight loss of samples after immersion was measured at 3, 7 and 14 d. The corrosion product on surface of samples was successively washed by chromic acid (200 g L^{-1} CrO$_3$ and 10 g L^{-1} AgNO$_3$) at room temperature, distilled water and ultrasonic wave for 10 min, and then was dried and weighed. The average corrosion rate was calculated by the following formula:

$$Corrosion\ rate = (K \times W)/(A \times T \times D) \tag{1}$$

where K is a constant, 8.76×10^4; W is the mass loss (g); A is the surface area of sample exposed to Hank's solution; T is the time of exposure (h); D is the density of material (g cm^{-3}).

After the immersion test, the samples were cleaned to remove the corrosion products on surfaces and their morphologies were examined using both optical and SEM.

2.3 Electrochemical Test

The samples with size of $\varphi 10$ mm × 10 mm were prepared for electrochemical test. Potentiodynamic polarization tests were carried out on an electrochemical workstation (Reference 600, Gamry, USA). A conventional three-electrode system was used for the tests, in which the sample was taken as the working electrode, a saturated calomel electrode as the reference electrode (SCE), and a

platinum electrode as the auxiliary electrode. All the tests were conducted in the Hank's solution at 37 ± 0.5 °C. The change in the open-circuit potential (OCP) was first monitored as a function of immersion time for about 30 min. Potentiodynamic polarizations were conducted on both cast- and heat-treated extruded Mg–Sr alloys, with an initial potential of − 0.25 V relative to the open-circuit potential and a scanning rate of 0.5 mV s^{-1}. The obtained results were analyzed by Tafel extrapolation method [24]. Electrochemical impedance spectroscopy (EIS) was measured at the open-circuit potential with an amplitude of 10 mV in the frequency range from 100 kHz to 10 mHz. Three parallel samples were used for each result to confirm the repeatability. The equivalent circuit was fitted using ZsimDemo software.

3 Results

3.1 Microstructure

3.1.1 As-Cast and As-Extruded Mg–1.5Sr Alloys

Figure 1a shows the optical microstructure of cast Mg–1.5Sr alloy, consisting of Mg matrix and second phases. There are braid-like bands with same orientation within grains, and the homogeneity of orientation is not damaged by the precipitation of second phases, as illustrated in Fig. 1b. It can be found from the line scan of energy-dispersive spectroscope (EDS) showing elemental distribution in the cast Mg–1.5Sr alloy, as shown in Fig. 1c and d, that Sr is mainly concentrated at grain boundary, and only few Sr is dissolved in the Mg matrix. However, oxygen (O) distributes on the whole surface of sample and the O content is largely increased at grain boundary where containing second phases. It has been reported that Sr is easier to combine with O to form dense oxide film [25].

Microstructures of the extruded Mg–1.5Sr alloy on transversal and longitudinal surfaces are shown in Fig. 2a and b. The average grain sizes of as-cast and as-extruded (transverse and longitude) Mg–1.5Sr alloys are shown in Fig. 3a. After extrusion, the grains were largely refined due to the occurrence of recrystallization, but the grain size was
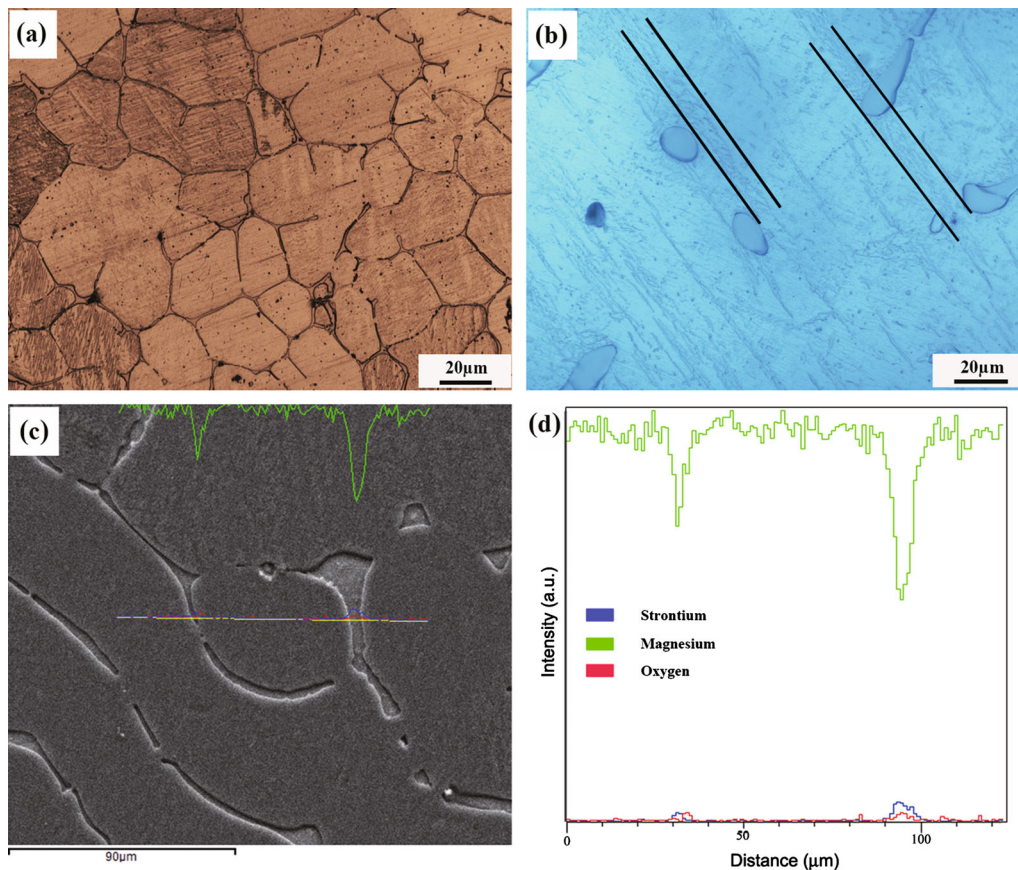
Fig. 1 Microstructures of as-cast Mg–Sr alloy: **a** optical micrograph, **b** higher magnification showing braid shape bands within grain, **c** SEM micrograph, **d** EDS line scan analyses

not uniform. The grain size of "ex-l" was slightly larger than "ex-t." The second phases that precipitated along grain boundaries in the cast alloy were broken, and those on the transversal surface randomly and unevenly distributed at grain boundaries and within grains, with different sizes and morphologies such as water drop-like, short rod-like and ball-like. However, the second phases on the longitudinal surface had a discontinuous banding distribution at grain boundaries along extrusion direction, mainly in strip-like morphology. The volume fractions of second phases on transversal and longitudinal surfaces of the extruded alloy are presented in Fig. 3b, showing that the later is a little bit higher than the former, which might be caused by the elongation of second phases on longitudinal direction from the extrusion. It can also be seen from XRD analysis shown in Fig. 4a that the as-cast Mg–1.5Sr alloy is composed of Mg matrix and β-$Mg_{17}Sr_2$, and there is no obvious change after extrusion. Higher peaks of some orientations can be found on the transverse and longitudinal sections of extruded Mg–Sr alloy, which indicates that the dynamic recrystallization happened along certain orientation after extrusion.

3.1.2 Extruded Mg–1.5Sr Alloy Under Different Heat Treatments

Transversal and longitudinal microstructures of the extruded Mg–1.5Sr alloy under different heat treatments are shown in Fig. 2. The average grain sizes in the alloy after different heat treatments are presented in Fig. 3a. The grain size of the alloy after 450 °C solution grew up greatly compared with that before the heat treatment. Increase in the solution temperature made a little growth of the grains. The grains did not clearly grow up after a short-term aging. However, when the aging time was extended to 24 h, grains grew up obviously. Continuing to increase the aging time made small change on the grain size. After the aging treatment, the grain size obviously became inhomogeneous. The second phases in the heat-treated Mg–1.5Sr alloy were counted under different views, and Fig. 3b shows volume fractions of second phases in different samples.

The variation of second phase after heat treatment is clearly shown in Fig. 5. Morphologies of second phases in the extruded Mg–1.5Sr alloy without heat treatment were not uniform, with different morphologies such as plate-
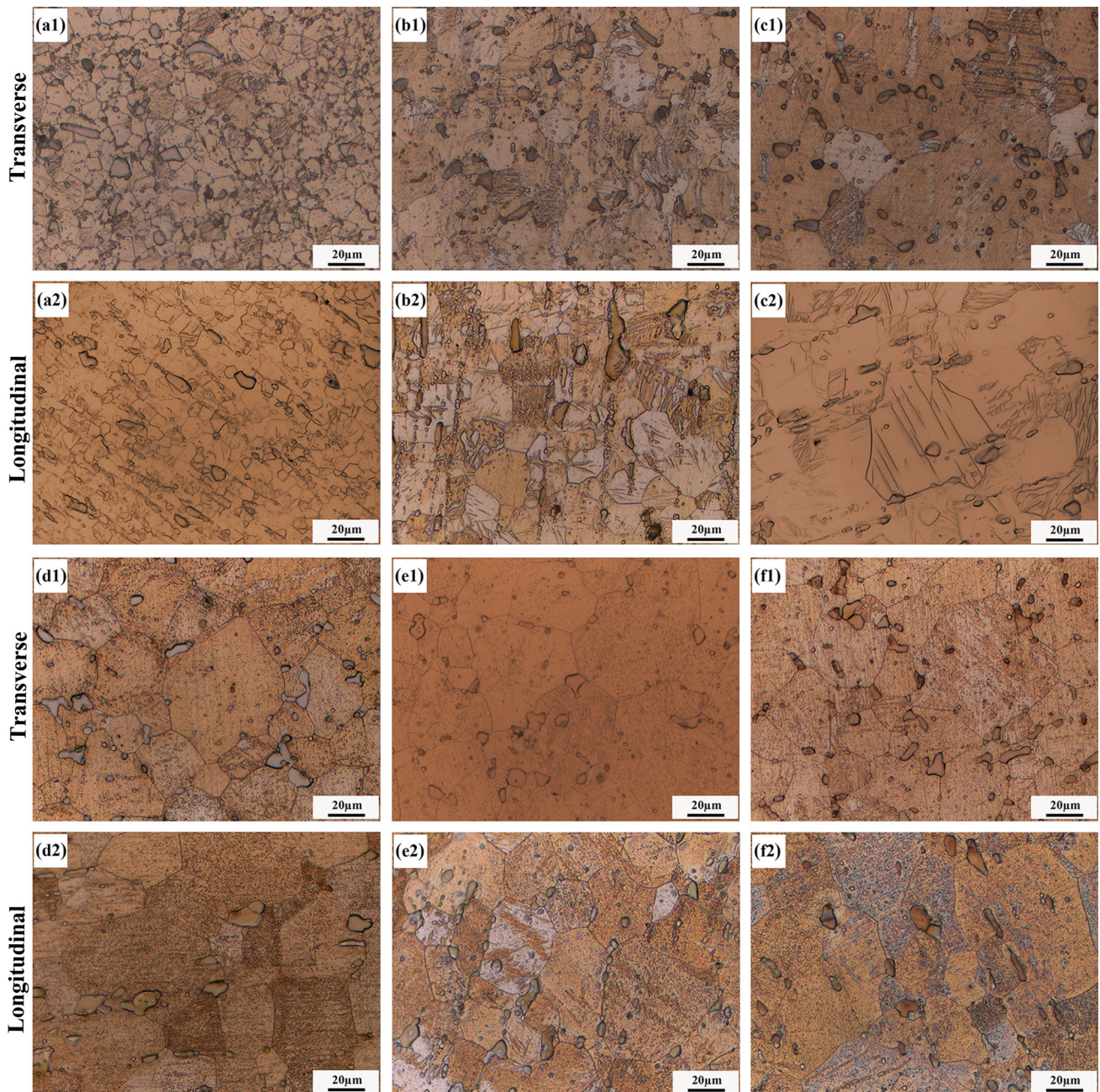
Fig. 2 Optical micrographs of as-extruded Mg–Sr alloy under different heat treatments shown by transversal and longitudinal sections: **a1** and **a2** before heat treatment, **b1** and **b2** T4-450 °C, **c1** and **c2** T4-560 °C, **d1** and **d2** T6-10 h, **e1** and **e2** T6-24 h, **f1** and **f2** T6-40 h

like, long rod-like and ball-like distributed within grains. After solution treatment for different time, the second phases were dissolved, the big plate-like second phases became smaller, but the large-sized second phases still existed with uniform distribution. However, after solution treatment at 560 °C, the second phases continued to be dissolved, and the big plate-like phases changed to the rod-like and ball-like phases. Since the second phases were dissolved too much, the complete dissolution into the

matrix happened in some areas, resulting in inhomogeneous distribution of second phases, as shown in Fig. 5c.

The alloy was aged after the solution treatment, and more second phases precipitated at grain boundaries and within grains. The connection easily happened among the second phases at grain boundaries, resulting in the interface to disappear and the formation of polygon plate-like second phases, which greatly influenced corrosion resistance of the alloy. However, fine and dispersed second phases precipitated within grains. As extending the aging time, more
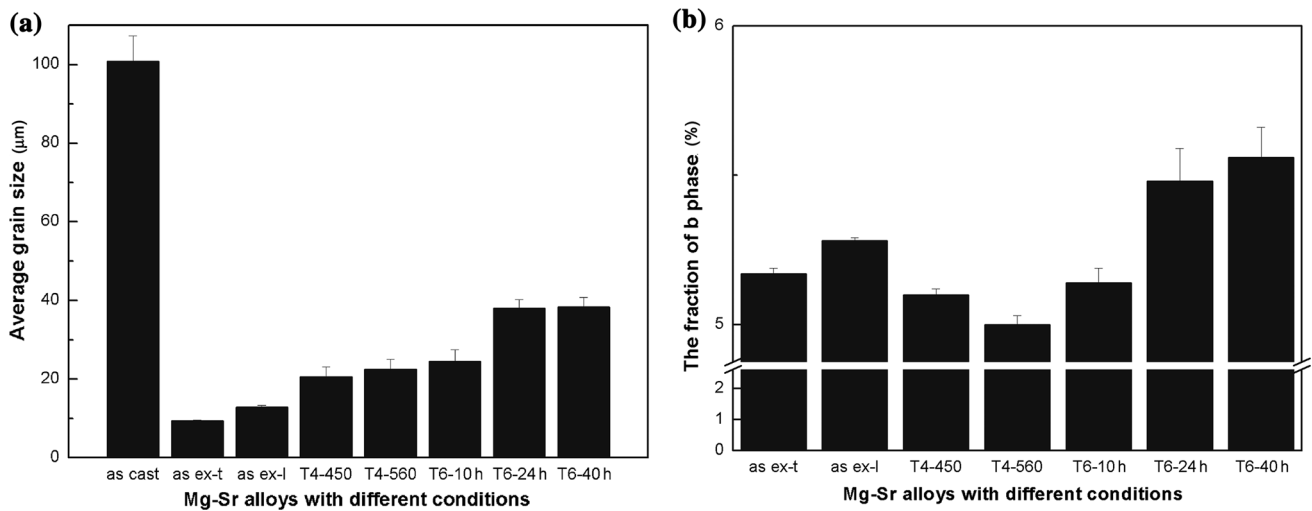
Fig. 3 a Average grain size and **b** volume fractions of β phase in cast and extruded Mg–1.5Sr alloy under different heat treatments
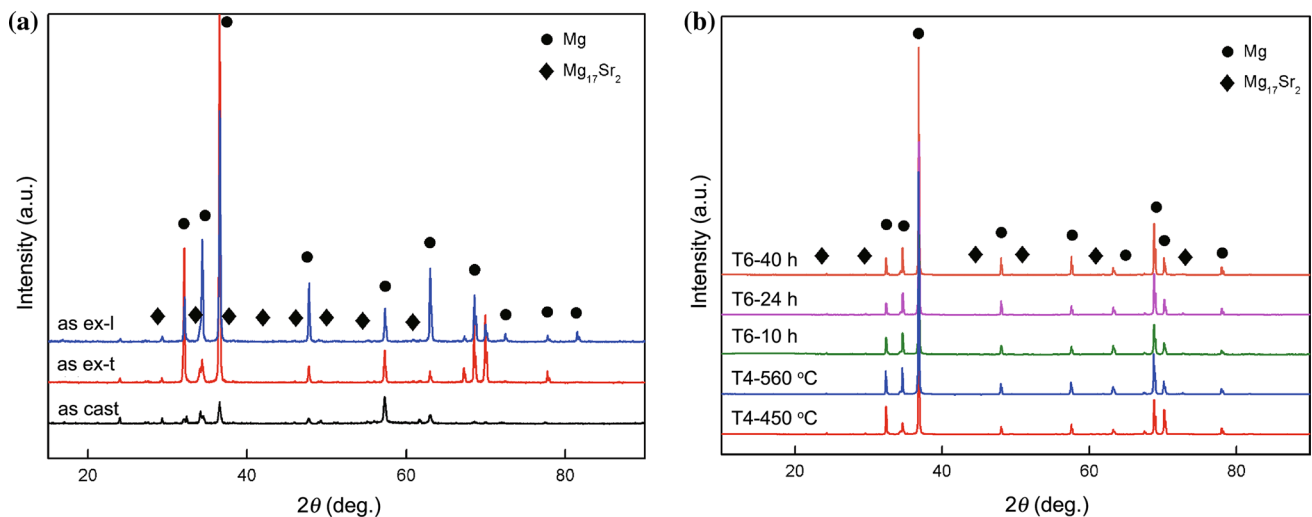

Fig. 4 XRD patterns of **a** as-cast, as-extruded Mg–Sr alloy and **b** under different heat treatments

second phases precipitated. Especially after 40-h aging, the second phases were seriously coarsened, even exhibiting banding distribution, as shown in Fig. 5f. X-ray diffraction (XRD) patterns of the extruded Mg–1.5Sr alloy subjected to different heat treatments are shown in Fig. 4b. The heat treatment had no effect on phase components in the extruded alloy, still consisting of Mg matrix and β-Mg$_{17}$-Sr$_2$ s phases with obvious textures. Due to only fewer amounts of second phases, the change in second phases could not be clearly found from the XRD results.

3.2 Immersion Test

3.2.1 Cast and Extruded Mg–1.5Sr Alloys

The cast and extruded (both transversal and longitudinal) Mg–1.5Sr alloy samples were immersed in Hank's

solution, and the variations of pH of the solutions are shown in Fig. 6. Hydroxyl will be produced when a magnesium alloy is immersed in the aqueous solution to form an alkaline environment. So the pH value can well reflect the corrosion resistance of the magnesium alloy. According to the changing tendency of pH, the corrosions of Mg–1.5Sr alloy in different states were in the following order from high to low: cast > extruded (longitudinal) > extruded (transversal). After 1-day immersions of cast and extruded (longitudinal) alloys, respectively, the pH increased from 7.4 to about 11, a little bit higher for the former. However, the pH for the extruded (transversal) alloy was only less than 10, showing better corrosion resistance. As increase in the immersion time, the pH for both cast and extruded (longitudinal) alloys presented a tendency of increasing firstly and then reaching steady state, i.e., accelerating the corrosion in the early stage and
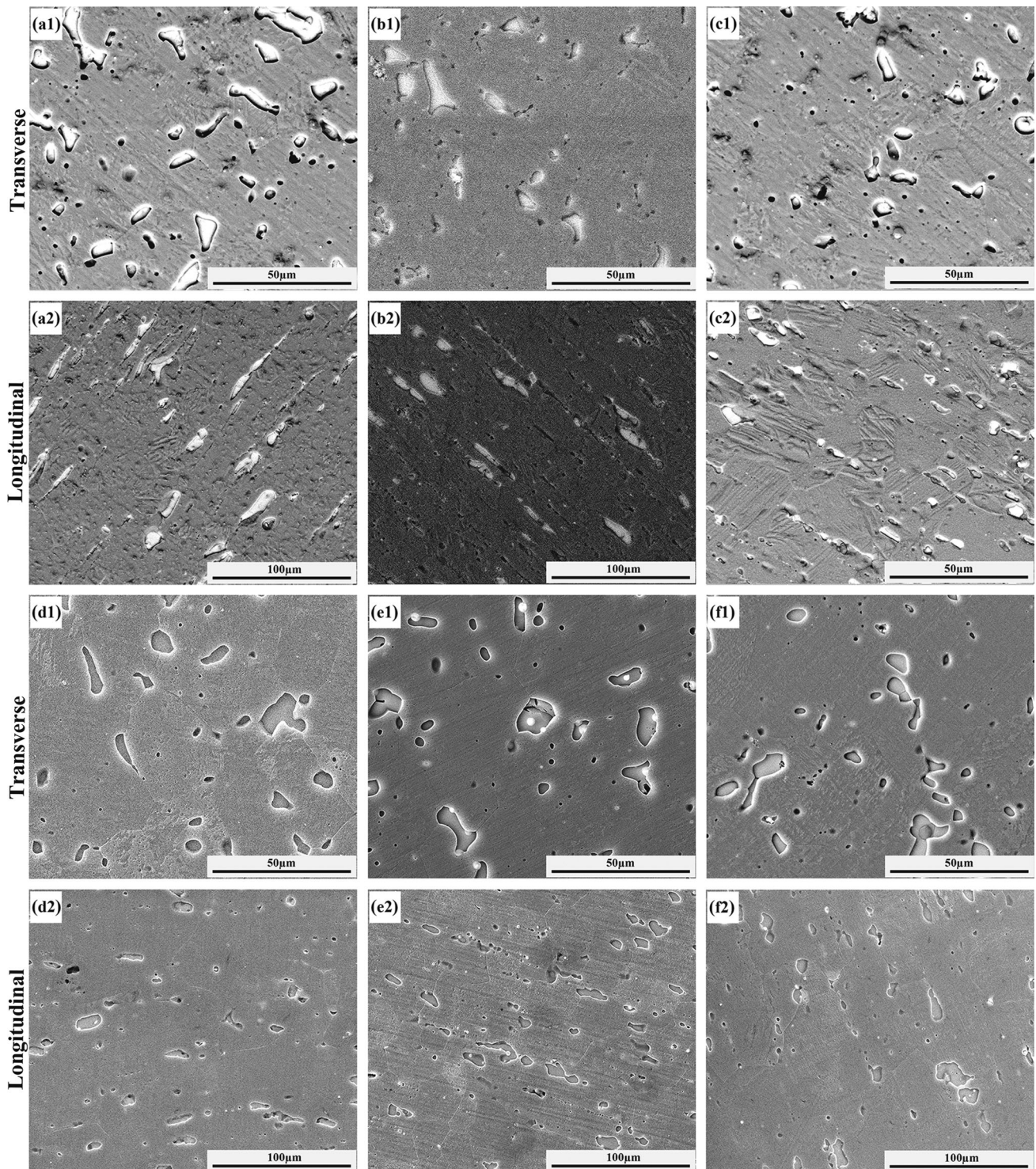
Fig. 5 SEM micrographs of as-extruded Mg–1.5Sr alloy under different heat treatments shown by transversal and longitudinal sections: **a1** and **a2** before heat treatment, **b1** and **b2** T4-450 °C, **c1** and **c2** T4-560 °C, **d1** and **d2** T6-10 h, **e1** and **e2** T6-24 h, **f1** and **f2** T6-40 h

then going to a balance for corrosion. But the pH for the extruded (transversal) alloy largely decreased, which might be related to the prevention role of the film formed on the alloy surface after immersion.

Figure 7 shows the surface morphologies of the samples with removal of corrosion products after immersions for 3 and 9 d, respectively. As shown in Fig. 7a1, the cast Mg–1.5Sr alloy mainly showed intergranular corrosion after 3-d immersion. The second phases at grain boundaries dropped
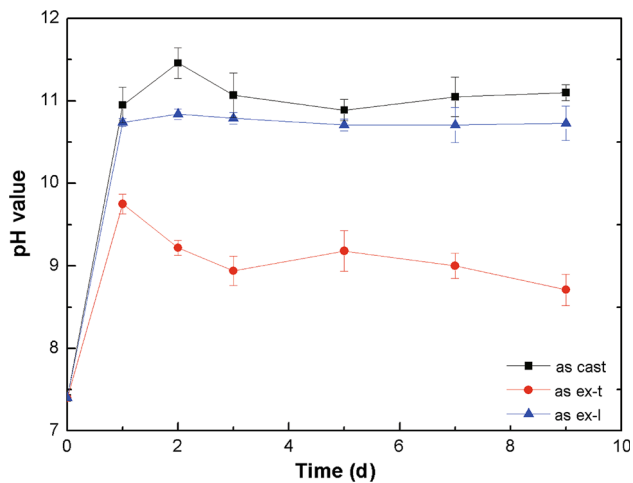
Fig. 6 Variation of pH value for as-cast and as-extruded Mg–1.5Sr alloy during immersion in Hank's solution for 9 d

off due to the corrosion, forming reticular trenches along grain boundaries, and only light uniform corrosion happened within grains. It can be seen from Fig. 8a1 with higher magnification that the corrosion within grains started from grain boundaries and propagated into grains with characteristic of filiform corrosion, but most of grains were not corroded. After 9-d immersion, large amount of corrosion occurred within grains. However, the transversal section of as-extruded Mg–1.5Sr alloy (Fig. 7b1 and b2)

corroded much less than the cast alloy. The corrosion happened slightly after 3-d immersion (Fig. 7b1), mainly as filiform and pitting corrosions, and no corrosion happened for the most of matrix. As the immersion time was extended (Fig. 7b2), the corrosion area was enlarged, but there still existed some areas without corrosion. In Fig. 7c1, it can be seen that after 3-d immersion, large area corrosion happened locally on the longitudinal section of extruded alloy characterized by filiform corrosion. This was related to the elongated second phases with banding distribution along grain boundaries in the longitudinal microstructure, and the linear arrangement of second phases accelerated the development of corrosion. After 9-d immersion (Fig. 7c2), it can be obviously found that the surface of the alloy was almost corroded, clearly seeing some corroded trenches with relatively same directions. Figure 7c2 shows that the corrosion did not continue to develop to the surrounding grains, more possibly connecting with the corrosion pits left by peeling off of the other second phases to form corrosion trenches shown by the arrows.

Figure 8b1 shows the corrosion morphology of the transversal section of as-extruded alloy after 3-d immersion. It can be seen that the surrounding of plate-like second phase was separated from the matrix due to the effect of galvanic corrosion, resulting in occurrence of the gap. It
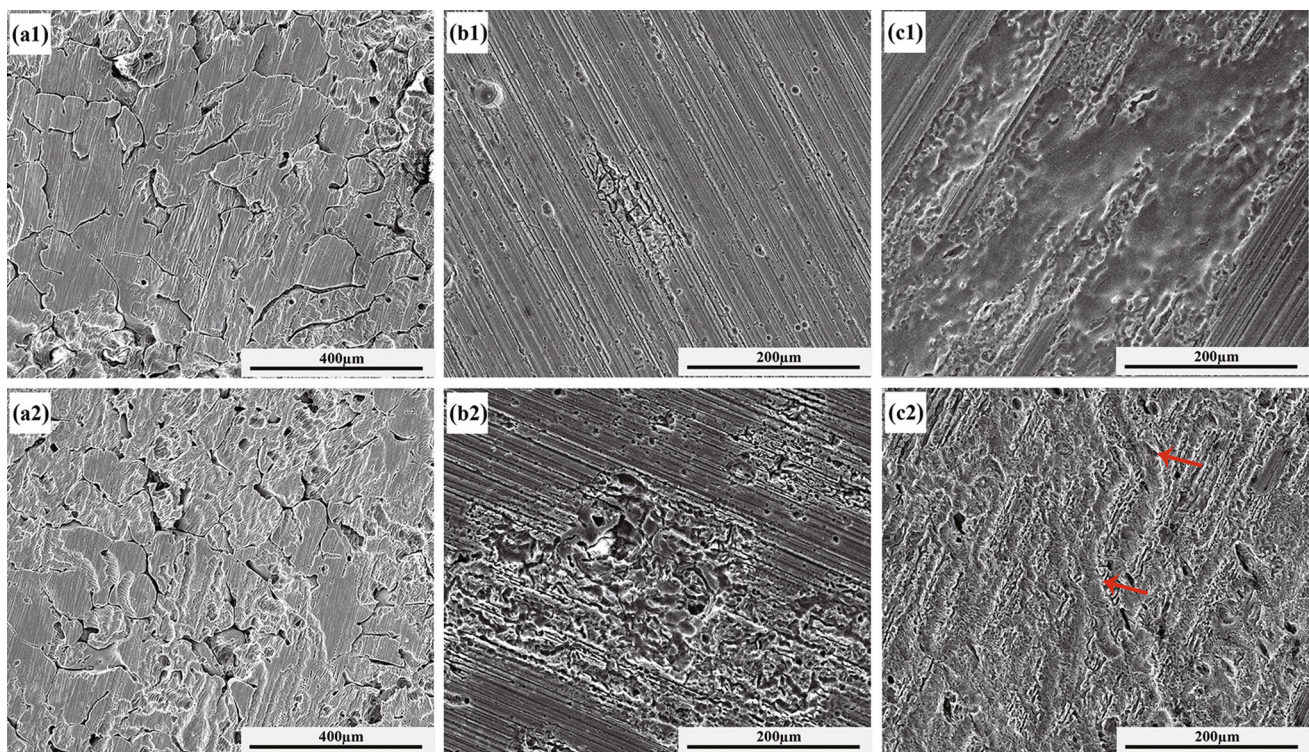

Fig. 7 SEM micrographs showing corroded surface of Mg–1.5Sr alloy immersed in Hank's solution for 3 d (**a1–c1**) and 9 d (**a2–b2**): **a1** and **a2** as-cast alloy, **b1** and **b2** transversal section as-extruded alloy, **c1** and **c2** longitudinal section of as-extruded alloy
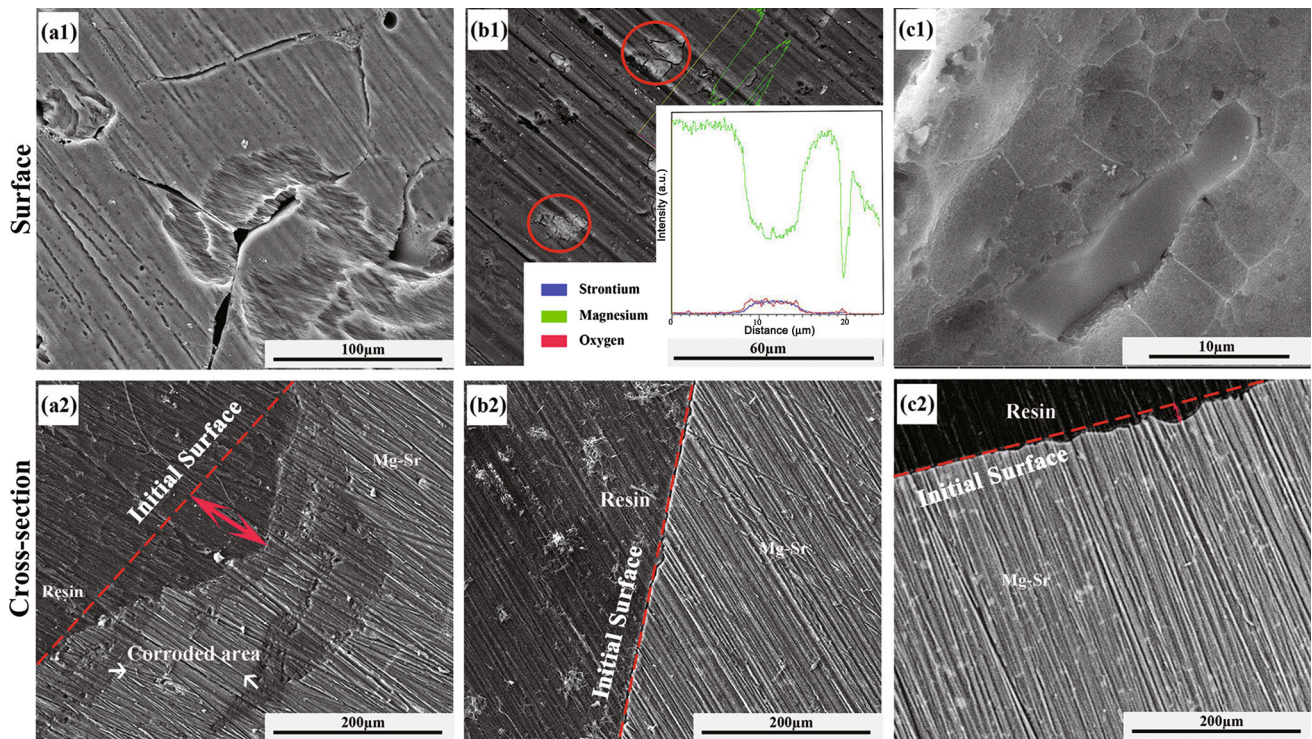
Fig. 8 SEM micrographs showing corrosion morphologies of β phase and cross sections of Mg–1.5Sr alloy exhibiting the depth of corrosion pit after 3-d immersion in Hank's solution: **a1** and **a2** as-cast alloy, **b1** and **b2** transversal section of as-extruded alloy, **c1** and **c2** longitudinal section

should be noted that cracking of β phase happened in Hank's solution, which is marked in circle. Figure 8c1 shows the corroded trenches with higher magnification after 3-d immersion. The rod-like second phases dropped off along grain boundaries during the corrosion.

Figure 8a2, b2 and c2 shows the corrosion morphologies of the cross sections of the cast, extruded (transversal) and extruded (longitudinal) Mg–1.5Sr alloys after 9-d immersion, respectively, the sides being covered with epoxy resin. The corrosion pits on the cast alloy were greatly larger than those on as ex-t (transversal) and as ex-l (longitudinal) alloys, which was related to the grain sizes of these states. The grain size in the cast alloy was relatively large, and after corrosion along grain boundaries to some extent, the grains peeled off, leaving relatively deep and wide corrosion pits. The development of corrosion for the cast alloy shown in Fig. 8a2 was not layer by layer, instead of selectively developing to certain direction by by-passing some matrix. This also verifies that after peeling off of the second phases at grain boundaries, the solution could enter into the deeper grains through the gaps left at grain boundaries. So the corrosion preferred to happen along grain boundaries without corrosion of grains. However, filiform and pitting corrosions mainly happened on the extruded alloy, and smaller grain size made relatively shallow and small corrosion pits. Corrosion pits on the as ex-t (transversal) alloy randomly distributed compared

with the as ex-l (longitudinal) alloy, showing continuous pits on the later.

3.2.2 Extruded Mg–1.5Sr Alloy Under Different Heat Treatments

Figure 9a shows the pH variations for the extruded Mg–1.5Sr alloys before and after heat treatment that were immersed for 14 d. The lowest pH was found for the extruded alloy after solution at 450 °C for 5 h, indicating the smallest degradation of the alloy. When the solution temperature was increased to 560 °C, the corrosion resistance became poor with pH, which was higher than the alloy before heat treatment. The 560 °C solutioned alloy was aged at 200 °C for 10, 24 and 40 h, respectively, and from the variation of pH, it can be seen that the pH of aged alloy was greatly higher than the alloy before aging, i.e., aging treatment promoted the degradation of the alloy. The longer the aging time was, the higher the pH value was.

The weight losses of the extruded Mg–1.5Sr alloys before and after heat treatment followed by immersion for 3, 7 and 14 d are shown in Fig. 9b. During the immersion, the alloy after solution at 450 °C for 5 h always had the lowest corrosion rate. The corrosion rates are ordered as the following: T4-450 °C < as-extruded < T4-560 °C < T6-10 h < T6-24 h < T6-40 h.
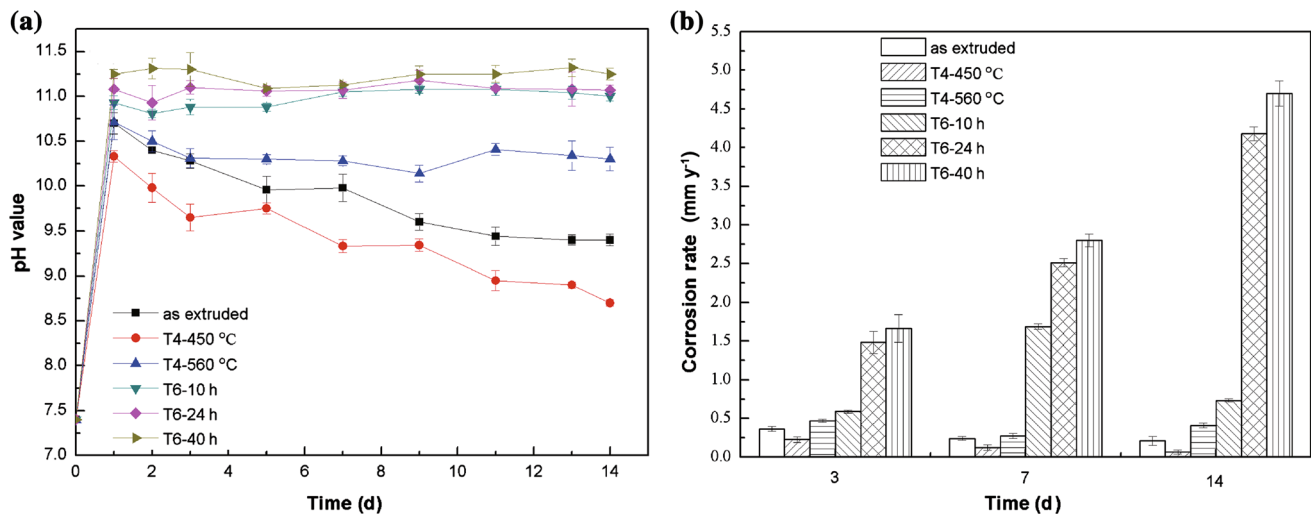
Fig. 9 **a** Variation of pH and **b** weight loss rate for extruded Mg–1.5Sr alloy under different heat treatments immersed in Hank's solution as a function of immersion time

Figure 10 shows the corrosion morphologies of the Mg–1.5Sr alloy after heat treatment that was immersed for 7 d. The extruded alloy mainly exhibited filiform and pitting corrosions. The local corrosion of alloy before heat treatment (Fig. 10a) was dominant by filiform and pitting corrosions, with some light uniform corrosion in the matrix for T4-450 °C alloy (Fig. 10b) and mainly filiform corrosion for T4-560 °C alloy (Fig. 10c) with uneven distribution, which was related to the unhomogeneous distribution of second phases in the microstructure. The surfaces of the alloys with solution and aging treatments were almost completely corroded. The corroded T6-10 h alloy (Fig. 10d) was covered by filiform corrosions, and as increase in the aging time, the samples were almost corroded into black color (Fig. 10e, f). The corrosions shown by the corrosion morphologies also agree well with the difference in corrosion rate mentioned above.
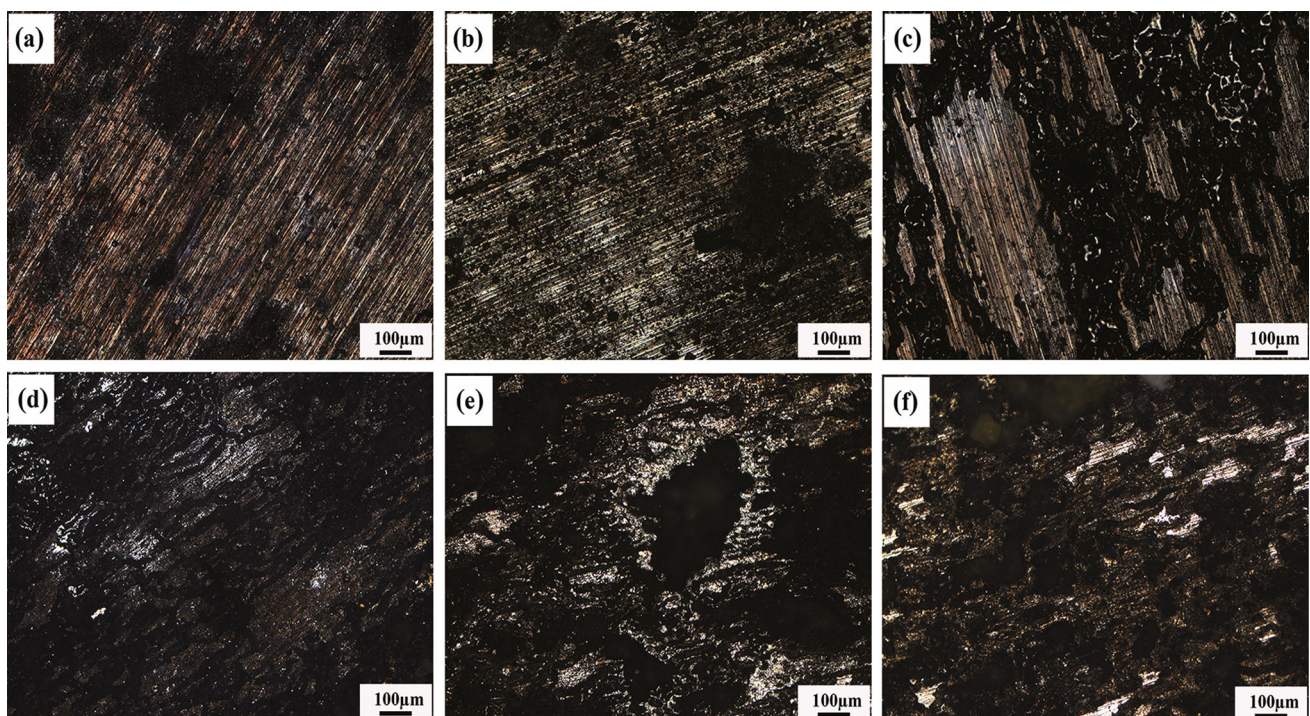

Fig. 10 Optical micrographs showing corrosion morphologies of extruded Mg–1.5Sr alloy under different heat treatments after 14-d immersion: **a** before heat treatment, **b** T4-450 °C, **c** T4-560 °C, **d** T6-10 h, **e** T6-24 h, **f** T6-40 h

3.3 Electrochemical Behaviors

3.3.1 As-Cast and As-Extruded Mg–1.5Sr Alloys

The electrochemical corrosion behavior of Mg–1.5Sr alloy in Hank's solution is shown in Fig. 11a. The corrosion potential (E_{corr}), Tafel gradient (β_c), corrosion current density (I_{corr}) and corrosion rate (CR) obtained by Tafel results are summarized in Table 2.

In Fig. 11a, it can be seen that after the extrusion both anode and cathode polarization curves of Mg–1.5Sr alloy were changed. The anode curve of the extruded alloy behaved obvious passivation characteristics, while the cast alloy behaved unremarkable in the solution. The corrosion rates obtained from fitting of the polarization curves are listed in Table 2, which is relatively consistent with the above immersion test results, i.e., hot extrusion could largely decrease the corrosion rate of Mg–1.5Sr alloy. The anode and cathode polarizations of as ex-t (transversal) and as ex-l (longitudinal) alloys were similar. However, the corrosion potential (E_{corr}) of the as ex-t (transversal) alloy was higher than that of the as ex-l (longitudinal), and its corrosion current (I_{corr}) was lower than that of the as ex-l (longitudinal). The decreasing tendency of corrosion resistance for three differently treated alloys is in the following order: as ex-t > as ex-l > as-cast.

Figure 11b and c shows the effect of solution and solution plus aging on the electrochemical behavior of the extruded Mg–1.5Sr alloy. In Table 2, it can be found that after solution at T4-450 °C for 5 h, the E_{corr} of extruded alloy was changed from − 1.63 to 1.60 V, and the I_{corr} decreased. Compared with T4-450 °C alloy and the alloy without heat treatment, as shown in Fig. 11b, the polarization curve of T4-560 °C alloy did not behave an obvious passivation feature, with the decrease in corrosion potential and the increase in corrosion current.

For the alloy solutioned at 560 °C for 5 h and followed by aging (Fig. 11c), as the aging time was extended, the E_{corr} decreased from − 1.64 V before aging to − 1.69 V after aging, I_{corr} increased from 4.31 to 8.98 μA cm^{-2}, and the corrosion rate was increased. It can be seen from the polarization curve that the heat treatment did not have obvious effect on cathode process of the alloy, but much affected the anode process, and then affected the degradation rate of the alloy. The result of polarization curve can be well connected with that of immersion test. The decreasing tendency of corrosion resistance of the alloy after heat treatment is ordered as the following: T4-450 °C > as-extruded > T4-560 °C > T6-10 h > T6-24 h > T6-40 h.

3.4 EIS Measurement

The EIS measurements of Mg–Sr alloy under different conditions were monitored in Hank's solutions after 1-h immersion, and the results are shown in Fig. 12. In all the cases, the results show three well-defined loops, containing one high-frequency capacitance loop, one medium-frequency capacitance loop and one low-frequency inductive loop. The loop diameters of different samples are different, suggesting that they have the same corrosion mechanism but different corrosion rates. In general, a larger diameter arc represents better corrosion resistance, so the corrosion resistance decreases in the following order: as ex-t > as ex-l > as cast and T4-450 °C > as-extruded > T4-560 °C > T6-10 h > T6-24 h > T6-40 h, obtained from Nyquist plots in Fig. 12a and b. The results agree well with the results obtained from both immersion test and potentiodynamic polarization test.

In order to further analyze the degradation behavior of the Mg–Sr alloy, the EIS spectra were analyzed and fitted using an equivalent circuit, $R_s(CPE1R_{tp})(CPE2R_{fp}(LR_L))$, with errors less than 10%, as shown in Fig. 12c. The fitted data are shown in Table 3. In this equivalent circuit, R_s represents the solution resistance, R_{tp} the charge transfer resistance, and CPE1 the capacitance, respectively. R_{fp} and
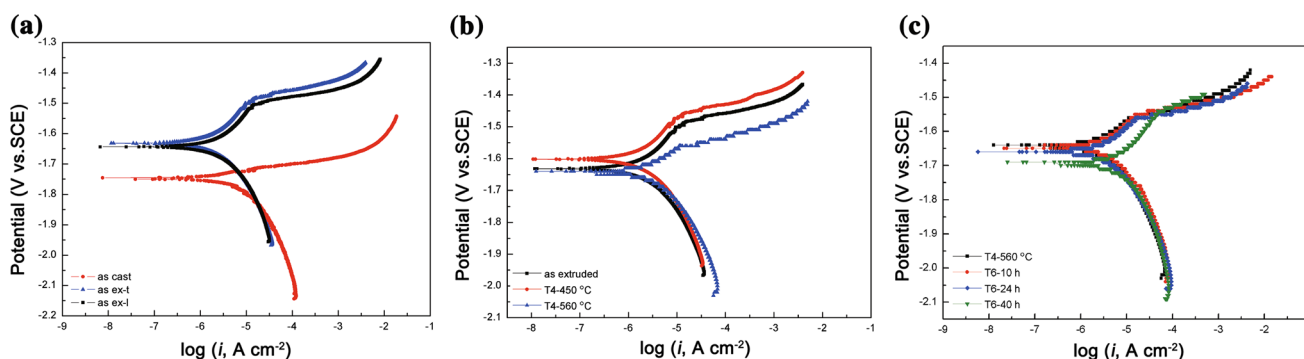

Fig. 11 Potentiodynamic polarization curves of Mg–1.5Sr alloy: **a** as-cast and as-extruded alloy, **b** solution-treated alloy, **c** solution followed by aging alloy

Table 2 E_{corr}, β_c and I_{corr} obtained from Tafel fitting for differently treated Mg–1.5Sr alloy in Hank's solution

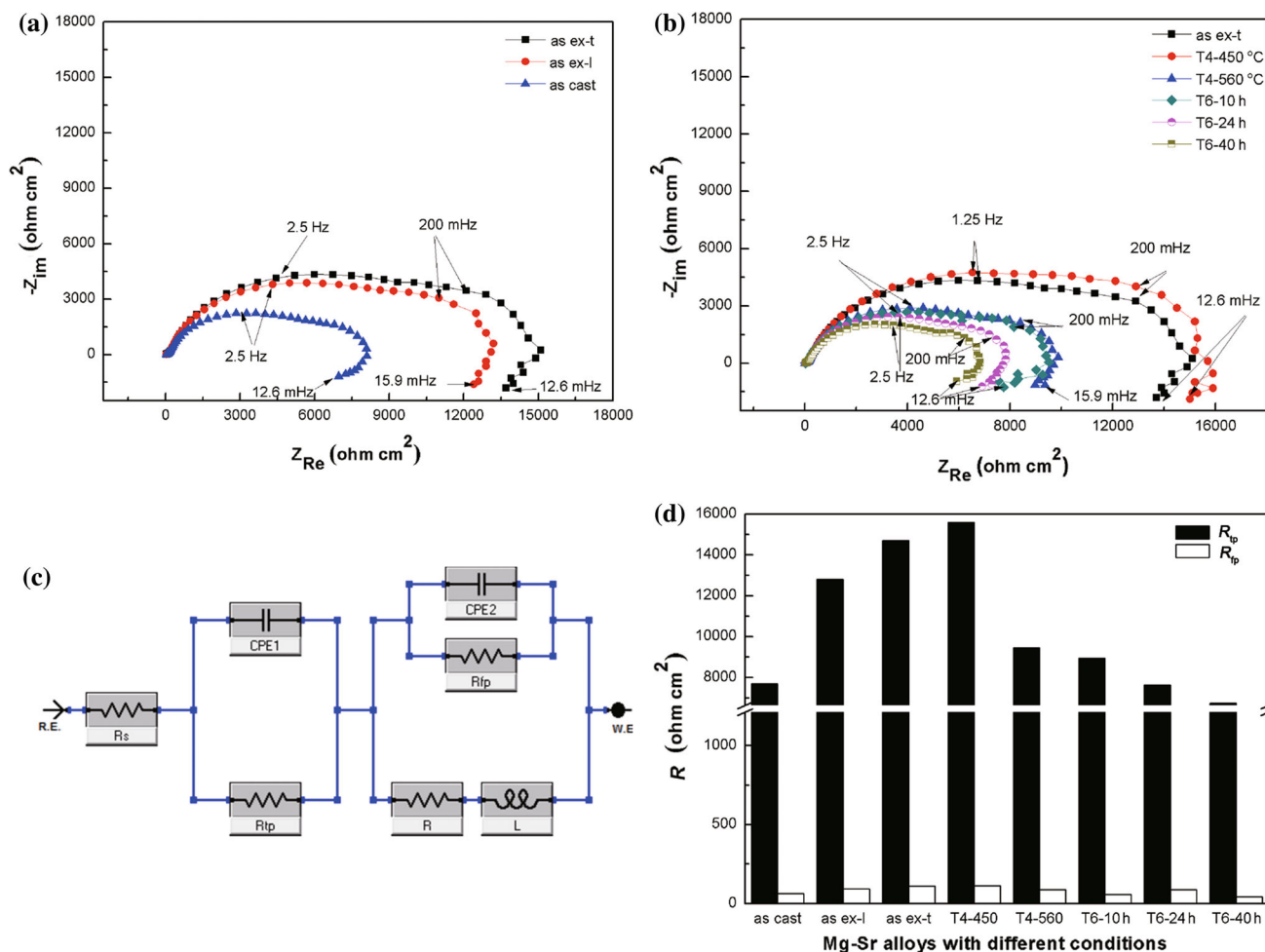| Sample	E_{corr} (V vs. SCE)	I_{corr} (µA cm^{-2})	β_c (V dec^{-1})	Corrosion rate (mm y^{-1})
As-cast	− 1.740	10.468	0.308	0.236
Ex-t	− 1.630	4.951	0.226	0.112
Ex-l	− 1.640	6.617	0.260	0.149
T4-450 °C	− 1.600	4.731	0.215	0.107
T4-560 °C	− 1.640	6.775	0.235	0.153
T6-10 h	− 1.650	7.702	0.201	0.174
T6-24 h	− 1.650	9.855	0.231	0.222
T6-40 h	− 1.690	14.115	0.194	0.318

Fig. 12 EIS measurement results of Mg–Sr alloy: **a** and **b** Nyquist plots acquired at 1-h immersion in Hank's solution, **c** equivalent circuit for EIS data fitting, **d** fitted R_{tp} and R_{fp} (Z_{Re}: real part of impedance; Z_{im}: imaginary part of impedance; R: impedance)

CPE2 indicate the resistance and the capacitance of the corrosion product layer. The CPE is normally defined by the n value (n is a dimensionless constant in the range $-1 \leq n \leq 1$, designated, for example, as n_1 and n_2 in Table 3). If n is equal to 1, CPE is identical to a capacitor. L and R_L indicate the inductance and the inductive resistance, respectively. The three loops in Nyquist plots suggest three time constants in the circuit, where the first one

(CPE1R_{tp}) at high frequency indicates that the charge transfer resistance at the interface of Mg–Sr alloy/electrolyte was associated with the micro-galvanic events. The second time constant (CPE2R_{fp}) at intermediate frequency is due to the diffusion of Mg^{2+} species through the corrosion layer, while the third time constant (LR_L) is related to the adsorption process. In general, a high value of R_{tp} indicates a lower degradation rate of Mg matrix. According

Table 3 Fitting results of Mg–Sr alloy immersed in Hank's for 1 h

Sample	R_s (Ω cm^{-2})	R_{tp} (Ω cm^{-2})	CPE1 (F cm^{-2})	n_1	R_{fp} (Ω cm^{-2})	CPE2 (F cm^{-2})	n_2	L (H cm^{-2})
As-cast	12.92	7689	2.20E−05	0.7425	62.19	1.02E−05	0.6977	10.60
Ex-t	15.57	1.47E + 04	1.76E−05	0.7657	113.00	3.09E−05	0.3911	17.69
Ex-l	12.02	1.28E + 04	1.61E−05	0.7362	91.92	3.58E−05	0.5732	18.36
T4-450 °C	13.14	1.56E + 04	1.66E−05	0.7662	110.5	1.43E−05	0.6578	29.72
T4-560 °C	14.58	9449	1.90E−05	0.7689	87.42	1.28E−05	0.6793	18.58
T6-10 h	17.1	8958	2.02E−05	0.7523	57.65	1.87E−05	0.6049	23.40
T6-24 h	10.09	7637	2.01E−05	0.7681	87.16	1.69E−05	0.652	21.63
T6-40 h	20.52	6750	2.41E−05	0.7288	43.50	4.46E−07	0.3635	25.78

to the fitted results shown in Table 3, the R_{tp} of Mg–1.5Sr alloy was significantly increased after extrusion and T4-450 °C treatment, implying that the electrochemical reaction was prevented on the interface. Larger R_{fp} indicates the formation of a more compact corrosion product on the Mg–Sr alloy surface. R_{fp} of the as-extruded Mg–Sr alloy is larger, suggesting that the corrosion film on the cast alloy was poorer than the extruded alloy. After heat treatment for the as-extruded alloy, the film protection of T4-450 °C alloy was increased a little, while T4-560 °C alloy was reduced significantly, which is consistent with the passivation characteristics in polarization curves. The variation trends of R_{tp} and R_{fp} are clearly shown in Fig. 12d. R_L and L in the circuit indicate the existence the metastable Mg^{2+} during the dissolution of the alloy, which is assumed to be due to the formation of the $MgO/Mg(OH)_2$ and an absorbed intermediate coverage, probably $Mg(OH)_{ads}^+$ or $Mg(OH)_2$ [26]. The presence of this inductance loop at the low frequency was attributed to some process of local corrosion, such as pitting process. In the present case, a thin film was formed and the local corrosion might easily be initiated in the presence of chloride ions, resulting in an uneven corrosion as shown in Fig. 10. The second phase might also fall off after the corrosion of second phase close to Mg matrix, resulting in more defects on the surface and leading to breakages of the corrosion layer.

4 Discussion

The present work studied the corrosion behaviors of Mg–1.5Sr alloy with different microstructures obtained by different processing approaches, and the results indicated that the microstructure of the alloy was changed mainly by grain size, as well as the size, quantity and distribution of the second phases.

4.1 Grain Size

The results of present study showed that the corrosion resistance of the extruded alloy with fine grains was much better than that of the cast alloy. The average size in the alloy under different conditions is ordered as the following: as-cast > T6-40 h > T6-24 h > T6-10 h > T4-560 °C > T4-450 °C > ex-l > ex-t, while the corrosion resistance can be ranked as the following decreasing order: as-cast < T6-40 h < T6-24 h < T6-10 h < T4-560 °C < ex-l < ex-t < T4-450 °C. Exception of the T4-450 °C alloy, the corrosion resistance of Mg–Sr alloy generally increased with the reduction in the grain size. The extrusion led to elongated grains at the longitudinal direction, which resulted in poor corrosion resistance compared with transversal direction.

At present, there were many arguments about the effect of grain boundary on the corrosion behavior of magnesium alloys. Aung and Zhou [13] pointed out that grain boundary in magnesium alloy could be a corrosion barrier to hinder the corrosion, while some other works considered that the grain boundary could be taken as a lattice defect to accelerate the corrosion. The present study immersed the extruded Mg–1.5Sr alloy, which presented grain boundaries after polishing and etching and then took it out. After removal of the corrosion product, the immersed sample was examined on optical microscope, as shown in Fig. 13. The filiform corrosion covered grains, and grain boundaries could not hinder the development of corrosion, instead that the corrosion preferred to develop along grain boundaries, as shown by arrows in the figure. So for the Mg–Sr alloy, the grain boundaries could not impede the corrosion extension. Study on AZ31 magnesium alloy by Liao et al. [14] also obtained similar results.

The effect of grain boundary on corrosion resistance of magnesium alloys should depend on the characteristic of the corrosion system. If the passivation film was formed in the corrosion process, the grain boundary could accelerate
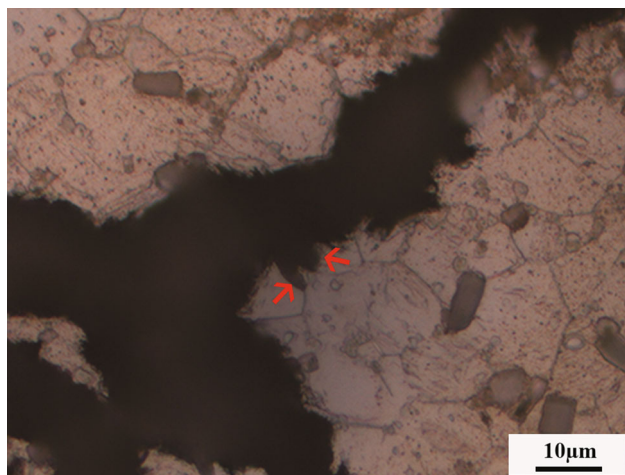
Fig. 13 Optical micrographs showing that grain boundaries could not stop corrosion process after 10 h immersion

the formation of more protective passivation film [15, 27]. In the present study, the electrochemical dissolution of Mg happened and thus accompanied by the production of OH^- ions as a result of H_2 formation from the cathodic reaction. The existence of OH^- ions resulted in the increase in pH and caused the formation and precipitation of $MgO/Mg(OH)_2$ as the corrosion products. At the interface of substrate and film layer, the Mg ions penetrated the film to form an outer layer of $Mg(OH)_2$, which was at the exterior surface of the film. Electrolytes in Hank's solution penetrated the film layer to form $Mg(OH)_2$ at the interior surface of the film. This process led to growth of the film layer [28]. However, the free volume mismatch between MgO layer and Mg substrate arose when the MgO was formed, causing a tensile stress in the MgO layer with possibility of cracking. A fine-grained microstructure most likely relived this stress by producing porosity through vacancy supply via grain boundaries [26]. In the present study, the EIS results and the fitted circuit implied that there was a film formed on the Mg–Sr alloy surface after immersion for a short time, indicated by the circuit parameters shown in Fig. 12. R_{fp} almost changed in the opposite trend to the grain size (Fig. 3a). In particular, as-extruded and T4-450 °C alloys showed much higher R_{tp} values. Thus, an initial MgO layer formed on surface of the fine-grained alloy provided better film coverage, and then, a more compact exterior $Mg(OH)_2$ layer formed, resulting in a better corrosion resistance.

4.2 Second Phases

The second phases in both cast and extruded Mg–1.5Sr alloys were all β-$Mg_{17}Sr_2$. Even though the standard electrode potential of $Mg_{17}Sr_2$ was not reported, the second phase should have different electrode potential with the Mg

matrix, which could be taken as the cathode of the galvanic corrosion [9]. In the present study, the distribution of second phases was changed through hot extrusion, and the quantity, size, and uniformity of second phases were also changed due to heat treatment of the extruded alloy. $Mg_{17}Sr_2$ had obvious effect on the corrosion of Mg–1.5Sr alloy, and the corrosion behavior was varied with different processing approaches.

The β phases had a continuous distribution along grain boundaries in the cast Mg–1.5Sr alloy, while the second phases redistributed after extrusion, randomly distributing at grain boundaries or within grains (Fig. 2). In general, the β phases with a net-like feature may act as a "barrier phase" to inhibit the overall corrosion of magnesium alloy [23]. Ambat et al. [29] and Ben-Haroush et al. [30] studied the cast and extruded AZ91 and AZ80 magnesium alloys, respectively, obtaining similar microstructures as the above. The results on corrosion rate indicated that corrosion resistances of AZ91 and AZ80 alloys decreased after extrusion, while it was increased for Mg–Sr alloy in the present work. In this study, the micro-galvanic corrosion happened between $Mg_{17}Sr_2$ and Mg matrix at first and formed intergranular corrosion. Figure 8b1 indicates that the corrosion cracking of β-$Mg_{17}Sr_2$ also happened during the immersion. The degradation of the matrix around second phase and the second phase itself resulted in dropping off of the reticular second phases, which was different from the results from the "barrier" mechanism. Zeng at el. [31] similarly reported that the fine precipitates along grain boundary would stimulate the grain boundary attack by acting as efficient local cathodes. Therefore, the second phases had no hindering effect on the corrosion of Mg–Sr alloy. The cast alloy with reticular second phases covered on all the grains of the cast microstructure had larger area ratio between anode and cathode compared with the fined second phases in the extruded alloy, thus resulting in more serious galvanic corrosion. Therefore, more Mg matrix in the cast Mg–1.5Sr alloy was corroded, showing higher alkaline, i.e., higher pH, in the early immersion period (Fig. 6). After drop off the corroded second phases from surface of the cast alloy, deep net-like gaps left among grains, making larger area exposure of grains below to the corrosive environment. The grains below started to corrode again from grain boundaries as the above mechanism, which continued in depth. A schematic corrosion mechanism of the as-cast Mg–1.5Sr is presented in Fig. 14a.

A proposed schematic corrosion mechanism of the as-extruded Mg–1.5Sr is shown in Fig. 14b. The $Mg_{17}Sr_2$ phase also could not hinder the corrosion process in the as-extruded alloy, so the micro-galvanic between the Mg matrix and $Mg_{17}Sr_2$ phase had dominated effect on the corrosion rate of Mg–Sr alloy. Results of T4-450 °C and T4-560 °C alloys showed that the volume fraction of β
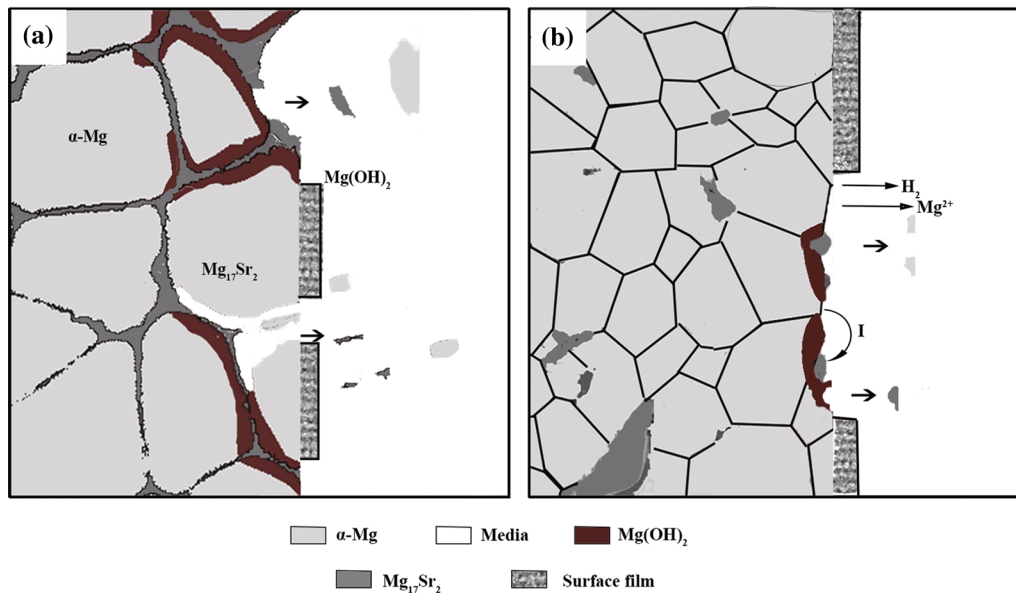
Legend:
■ α-Mg □ Media ■ Mg(OH)₂
■ Mg₁₇Sr₂ ▨ Surface film

Fig. 14 Schematic diagrams for corrosion mechanism of Mg–Sr alloy: **a** as-cast alloy, **b** as-extruded alloy

phases was all reduced, with more reduction in the microstructure of T4-560 °C alloy, resulting in more reduction of the galvanic corrosion, and thus, their corrosion resistances should decrease. However, the corrosion resistance of T4-450 °C alloy was better than that of the extruded alloy without heat treatment, while the corrosion resistance of T4-560 °C alloy was even worse, as shown in Fig. 9. This needs to be synthetically considered from the following factors: (1) the effect of grain size; (2) the amount and the distribution of second phases.

As the distance among second phases was not so large and homogeneous, relatively continuous passivation film could be formed [29]. More second phases were dissolved into the matrix of T4-560 °C alloy, resulting in inhomogeneous distribution of second phases (Fig. 5c). But the distribution of second phases in T4-450 °C alloy was relatively uniform, and the distance among second phases was less than that in T4-560 °C alloy. At the initial stage of degradation, some sites preferred to be attacked such as the matrix around second phases because of the micro-galvanic effect. The process of the film formation on the alloy surface was already mentioned, and R_{fp} values of T4-450 °C and T4-560 °C alloys also showed the relationship between the surface layer and second phases, although the effect of grain size should also be considered. However, the abnormal increase in R_{tp} of T6-24 h alloy should be noticed (Fig. 12d). This may also be attributed to the distribution of Mg₁₇Sr₂ phases, resulting in a more protective corrosion layer on the surface of alloy.

5 Conclusions

Mg–1.5Sr alloys with different microstructural characteristics were obtained through hot extrusion and followed by different heat treatments, and their effects on corrosion behavior of the alloy were investigated. The following conclusions are drawn from the study:

1. The corrosion behavior of Mg–Sr alloy was greatly related to its microstructure. The larger the grain size in the alloy was, the worse the corrosion resistance was. The alloy with fined grains formed a more protective surface film, bringing a better corrosion resistance.

2. The β-Mg₁₇Sr₂ s phases in Mg–Sr alloy corroded and cracked in Hank's solution, playing no effective obstacle role to the Mg matrix. The reticular distributed second phases in the cast alloy covered all the grains, and the serious galvanic corrosion resulted in much poor corrosion resistance of the alloy, mainly showing as the intergranular corrosion. The second phases in the extruded alloy were broken, reducing the galvanic corrosion and mainly showing as the filiform and pitting corrosions.

3. Solution at 450 °C for 5 h to the extruded Mg–1.5Sr alloy could effectively increase its corrosion resistance, but aging treatment could reduce the corrosion resistance of the alloy. The effects of both grain size and second phases should be comprehensively considered for corrosion behavior of the alloy.

References

[1] N. Li, Y. Zheng, J. Mater. Sci. Technol. **6**, 489 (2013)

[2] M.P. Staiger, A.M. Pietak, J. Huadmai, G. Dias, Biomaterials **9**, 1728 (2006)

[3] Y. Zhang, J. Xu, Y.C. Ruan, M.K. Yu, M. O'Laughlin, H. Wise, D. Chen, L. Tian, D. Shi, J. Wang, S. Chen, J.Q. Feng, D.H.K. Chow, X. Xie, L. Zheng, L. Huang, S. Huang, K. Leung, N. Lu, L. Zhao, H. Li, D. Zhao, X. Guo, K. Chan, F. Witte, H.C. Chan, Y. Zheng, L. Qin, Nat. Med. **10**, 1160 (2016)

[4] B. Solomon, R. Koppel, J. Jossiphov, Brain Res. Bull. **253**, 55 (2001)

[5] Y. Nakamura, Y. Tsumura, Y. Tonogai, T. Shibata, Y. Ito, Fundam. Appl. Toxicol. **2**, 106 (1997)

[6] S.P. Nielsen, Bone **3**, 583 (2004)

[7] Y. Fan, G.H. Wu, C.Q. Zhai, Mater. Sci. Forum **546–549**, 567 (2007)

[8] C. Liu, P. Wan, L.L. Tan, K. Wang, K. Yang, J. Orthop. Transl. **3**, 139 (2014)

[9] X.N. Gu, X.H. Xie, N. Li, Y.F. Zheng, L. Qin, Acta Biomater. **6**, 2360 (2012)

[10] Z. Li, X. Gu, S. Lou, Y. Zheng, Biomaterials **10**, 1329 (2008)

[11] L. Xu, G. Yu, E. Zhang, F. Pan, K. Yang, J. Biomed. Mater. Res. A **3**, 703 (2007)

[12] G.L. Song, A. Atrens, M. Dargusch, Corros. Sci. **4**, 1696 (2007)

[13] N.N. Aung, W. Zhou, Corros. Sci. **2**, 589 (2010)

[14] J. Liao, M. Hotta, N. Yamamoto, Corros. Sci. **61**, 208 (2012)

[15] K.D. Ralston, N. Birbilis, Corrosion **66**, 319 (2010)

[16] K.D. Ralston, G. Williams, N. Birbilis, Corrosion **6**, 507 (2012)

[17] R.C. Zeng, L. Sun, Y.F. Zheng, H.Z. Cui, E.H. Han, Corros. Sci. **69**, 79 (2014)

[18] S. Mathieu, C. Rapin, J. Steinmetz, P. Steinmetz, Corros. Sci. **12**, 2741 (2003)

[19] C. Scharf, A. Ditze, A. Shkurankov, E. Morales, C. Blawert, W. Dietzel, K.U. Kainer, Adv. Eng. Mater. **12**, 1134 (2005)

[20] G.L. Song, A. Atrens, X. Wu, B. Zhang, Corros. Sci. **10**, 1769 (1998)

[21] T. Zhang, Y. Li, F.H. Wang, Corros. Sci. **5**, 1249 (2006)

[22] M.C. Zhao, M. Liu, G. Song, A. Atrens, Corros. Sci. **7**, 1939 (2008)

[23] G.L. Song, A. Atrens, M. Dargusch, Corros. Sci. **2**, 249 (1998)

[24] E. McCafferty, Corros. Sci. **12**, 3202 (2005)

[25] Z. Feng, Q. Shi, X. Wang, L. Chen, Z.C. Xu, J. Dong, Y. Yang, J. Funct. Mater. **47**, 8124 (2016)

[26] K.Y. Chiu, M.H. Wong, F.T. Cheng, H.C. Man, Surf. Coat. Technol. **202**, 590 (2007)

[27] D. Orlov, K.D. Ralston, N. Birbilis, Y. Estrin, Acta Biomater. **15**, 6176 (2011)

[28] C.N. Cao, *Principle of Corrosion Electrochemistry* (Chemistry Industry Press, Beijing, 2004). **(in Chinese)**

[29] R. Ambat, N.N. Aung, W. Zhou, Corros. Sci. **8**, 1433 (2000)

[30] M. Ben-Haroush, G. Ben-Hamu, D. Eliezer, L. Wagner, Corros. Sci. **6**, 1766 (2008)

[31] R.C. Zeng, K.U. Kainer, C. Blawert, W. Dietzel, J. Alloys Compd. **509**, 4462 (2011)